IEEE Access
Multidisciplinary | Rapid Review | Open Access Journal

Received June 18, 2019, accepted June 28, 2019, date of publication July 10, 2019, date of current version July 31, 2019.

Digital Object Identifier 10.1109/ACCESS.2019.2928050

A New Mechanical Resonance Suppression Method for Large Optical Telescope by Using Nonlinear Active Disturbance Rejection Control

XIN LI[1,2], WENLIN ZHOU[1], JUN LUO[1], JUNZHANG QIAN[1], WENLI MA[1], PING JIANG[1], AND YONGKUN FAN[3]

[1]Institute of Optics and Electronics, Chinese Academy of Sciences, Chengdu 610209, China
[2]University of Chinese Academy of Sciences, Beijing 100049, China
[3]Sichuan Vocational and Technical College of Communications, Chengdu 611130, China

Corresponding author: Wenli Ma (mawenli@ioe.ac.cn)

This work was supported in part by the National Natural Science Foundation (NSFC) of China under Project 60978050, and in part by the Graduate Student Innovational Foundation of the Institute of Optics and Electronics, University of Chinese Academy of Sciences, under Project C12K011.

ABSTRACT Aiming at solving the problem of the multi-low-frequency mechanical resonances appearing in the large optical telescope control system, this paper proposes a novel control method based on nonlinear active disturbance rejection control (NADRC) and proportional–integral (PI) control. In the proposed control framework, a nonlinear tracking differentiator (NTD)-based feedforward control is designed to improve the tracking performance of the system. Then, the principle of suppression of mechanical resonance of this method is analyzed. Compared with the most commonly used acceleration feedback control (AFC) method, the theoretical analysis shows that the proposed method is more effective for suppressing the low-frequency mechanical resonance. Finally, the proposed method is applied to a large optical telescope, and the experimental results show that the proposed method is better than AFC.

INDEX TERMS Mechanical resonance suppression, active disturbance rejection control (ADRC), acceleration feedback control (AFC), nonlinear tracking differentiator (NTD), optical telescope.

I. INTRODUCTION

The large optical telescope is a kind of high precision observing equipment, and a high precision motion control system is essential. However, the tracking precision of the control system is affected by various known and unknown disturbances, such as mechanical resonance [1], friction torque [2], wind disturbance torque [3], [4], dead zone [1], un-modeled dynamics, etc. Among these disadvantages, the mechanical resonance which limits the bandwidth of speed has a serious impact, and the problem of mechanical resonance in the large telescope control system is a long-standing problem.

In [5], the low frequency mechanical resonance suppression methods that commonly used in industrial are explored, including low-pass filter method, notch filter method, Bi-quad filter method, etc. Unfortunately, these suppression methods are not suitable for large telescope. Because the mechanical resonance of large telescope has the following characteristics: 1) The resonant frequency is very low, generally lower than 50 Hz, sometimes even only a few Hz [6]. 2) The inertia ratio of the load and motor is very large [7]. 3) The damping ratio is small which means that the magnitude of the Bode diagram of the plant increases to very high levels at the nature frequency [3]. 4) There are usually multi low frequency resonances in the system [9]. 5) The system contains a variety of nonlinearities: friction, backlash, rate, and acceleration limits [7]. For the above reasons, the commonly used methods for suppressing resonance in large telescopes include: limiting the speed loop bandwidth, AFC [6], Quantitative Feedback Theory (QFT) [1], and linear-quadratic-Gaussian (LQG) [2], [3]. Among them, AFC is one of the most widely used methods, and it is used in many large telescopes to suppress mechanical resonance [6], [8]–[13].

In recent years, ADRC is used to suppress the mechanical resonance, and it takes the mechanical resonance as a disturbance and compensates the disturbance by extended

The associate editor coordinating the review of this manuscript and approving it for publication was Lei Wang.

state observer (ESO). In [14], [15], the performance of ADRC is better than AFC through extensive simulation and experimental results, however, the theoretical analysis was not conducted. In [16], [17], Model-based ADRC and non-model-based ADRC is used to control a two-mass benchmark problem, further demonstrating that ADRC has a good suppression performance for mechanical resonance. Reference [18] analyzes and proves that ADRC can compensate for mismatched disturbances, and give the principle of mechanical resonance suppression by using ADRC from the perspective of time domain. However, the physical meaning of how the ADRC suppresses mechanical resonance is not clear enough in time domain. Meanwhile, the linear extended state observer (LESO) of the linear active disturbance rejection control (LADRC) brings phase loss or sacrifices the nonlinear performance when the bandwidth of LESO is limited [19]–[21]. The nonlinear extended state observer (NESO) of NADRC has high observe efficiency [22], which reduces the phase loss, but is not widely used.

Considering the above problems, the following researches are carried out in this paper: 1) A composite control frame which includes NADRC (speed loop), PI (position loop) and NTD (speed and acceleration feedforward) is introduced to solve the problem of multi low frequency mechanical resonances in large telescope. 2) The mechanism of ADRC restraining mechanical resonance is studied from frequency domain perspective. 3) By comparing with AFC method, the advantages of suppressing low frequency mechanical resonance by using ADRC are explored. 4) The experimental results carried on a large optical telescope are presented to verify the correctness of the theoretical analysis and the effectiveness of the proposed method.

The rest of this paper is organized as follows. In section II, the model of the large telescope is analyzed, and a simplified model is deduced. In section III, the composite control method is proposed, the stability of the proposed method is proved, the resonance suppression mechanism of the method is discussed, and then the advantages of this method are illustrated by comparing with AFC. In section IV, experimental results are shown. In section V, concluding remarks are included.

II. MATHEMATICAL MODEL OF A LARGE TELESCOPE

Figure 1 shows the three-dimensional (3-D) sketch of a large optical telescope. Usually, the elastic deformation of the transmission mechanism cannot be neglected due to the excessive load, and this deformation will lead to deviation and lag in the transmission process, so the load cannot be regarded as an ideal rigid body. Fig. 2 shows the azimuth axis frequency response data (FRD) model of a large optical telescope, which has a low frequency resonance at 31Hz and 40Hz respectively. The FRD model varies according to the azimuth and elevation angles, friction, speed, and acceleration [1]. These nonlinearities and parameter uncertainties increase the difficulty of system analyzing

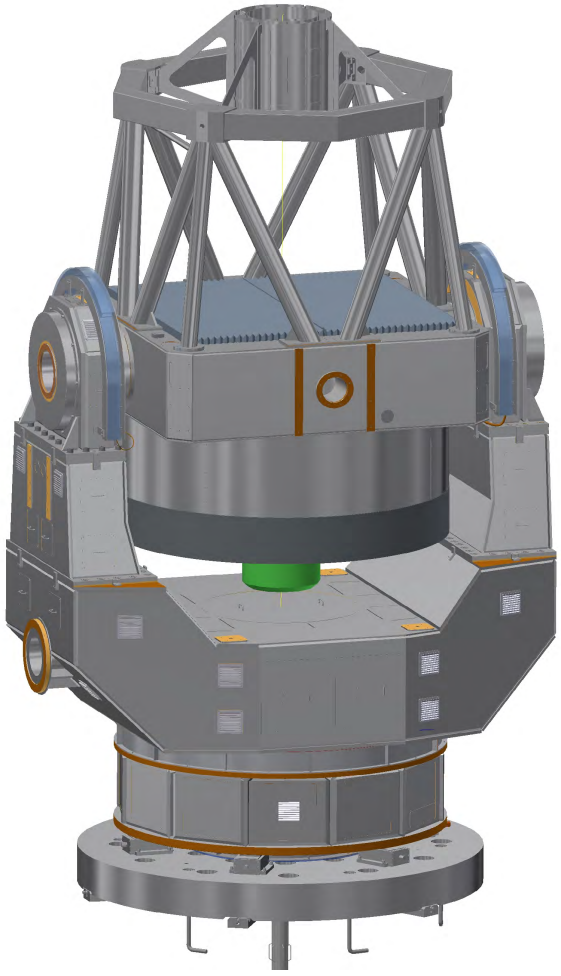

FIGURE 1. The 3-D sketch of a large optical telescope.

and design [1], [23].The compliant couple of the motor and the load in the telescope can be modeled as a two-inertia model as shown in Fig.3, and the feedback is a motor-side feedback [24].The inertia of the motor is J_M, the inertia of the load is J_L, the motor is connected to the load by a shaft, the stiffness coefficient is K_s, the damping coefficient is b_s, the electromagnetic torque of the motor is T_M, the load torque produced by the friction and wind disturbance is T_L and in most cases T_L is small, ω_M and θ_M represent the speed and angle of the motor, ω_L and θ_L represent the speed and angle of the load. The kinematics equations of the system shown in Fig.3 can be expressed as

$$\begin{cases} J_M\dot{\omega}_M = T_M - b_s(\omega_M - \omega_L) - K_s(\theta_M - \theta_L) \\ J_L\dot{\omega}_L = b_s(\omega_M - \omega_L) + K_s(\theta_M - \theta_L) - T_L \\ \omega_M = \dot{\theta}_M \\ \omega_L = \dot{\theta}_L \end{cases} \tag{1}$$

Then, the block diagram of the two-inertia model can be obtained as Fig.4. By ignoring T_L, the transfer function from

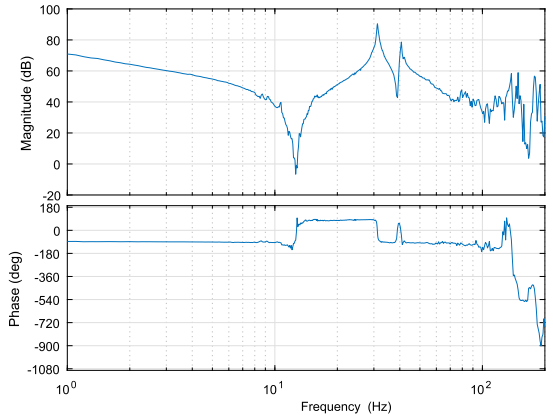

FIGURE 2. Measured telescope FRD model (from reference current I_{ref} to motor speed ω_M).

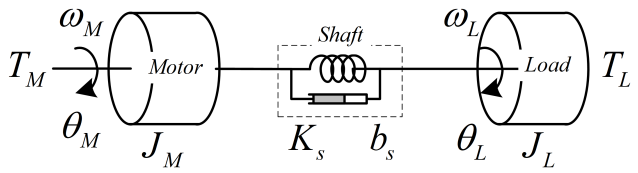

FIGURE 3. Two-inertia model.

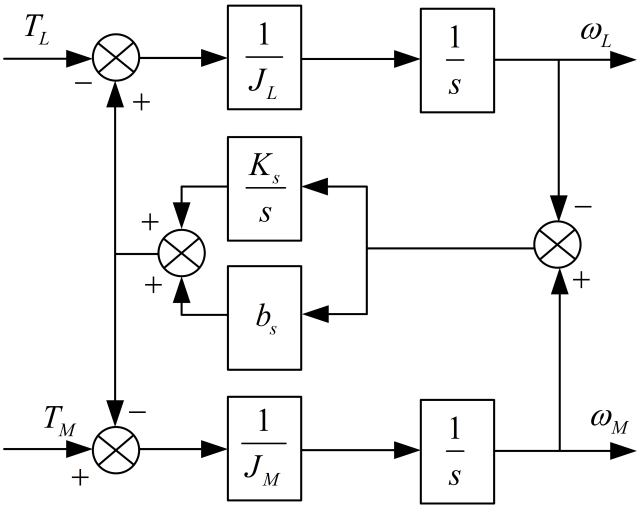

FIGURE 4. Block diagram of two-inertia model.

T_M to ω_M can be described as

$$G_{Model}(s) = \frac{\omega_M}{T_M} = \frac{1}{(J_M + J_L)} \cdot \frac{1}{s} \cdot \frac{J_L s^2 + b_s s + K_s}{\frac{J_M J_L}{(J_M + J_L)} s^2 + b_s s + K_s} \tag{2}$$

Usually, the motor current close loop can be regarded as (3) [24], k_T represents the torque coefficient of the motor, T_f is the time constant of the current close loop, I_{ref} is current reference, and in most cases, T_f is very small and can be ignored.

$$G_{acr}(s) = \frac{T_M}{I_{ref}} = \frac{k_T}{(T_f s + 1)^2} \tag{3}$$

Substitute (3) into (2), the transfer function from I_{ref} to ω_M can be induced

$$\begin{aligned} G_{Plant}(s) &= \frac{\omega_M}{I_{ref}} = G_{Model} \cdot G_{ASR} \\ &= \frac{1}{(T_f s + 1)^2} \cdot \frac{k_T}{(J_M + J_L)} \cdot \frac{1}{s} \cdot \frac{J_L s^2 + b_s s + K_s}{\frac{J_M J_L}{(J_M + J_L)} s^2 + b_s s + K_s} \end{aligned} \tag{4}$$

Let

$$G_1(s) = \frac{1}{s} \cdot \frac{1}{(T_f s + 1)^2} \tag{5}$$

$$G_2(s) = \frac{k_T}{(J_M + J_L)} \cdot \frac{J_L s^2 + b_s s + K_s}{\frac{J_M J_L}{(J_M + J_L)} s^2 + b_s s + K_s} \tag{6}$$

$G_1(s)$ is an ideal rigid body, whereas $G_2(s)$ is a compliance of the transmission component, which corrupts the ideal plant. The anti-resonant frequency (ω_A) and resonant frequency (ω_N) of the system can be calculated as

$$\begin{cases} \omega_A = \sqrt{\dfrac{K_s}{J_L}} \\ \omega_N = \sqrt{\dfrac{K_s}{J_L} + \dfrac{K_s}{J_M}} \end{cases} \tag{7}$$

When in the low frequency band, $s \to 0$, so $G_2(s) \approx k_T / (J_M + J_L)$, (4) can be simplified to (8), in this case the system is equivalent to a rigid body.

$$G'_{Plant}(s) = l_1(s) = \frac{1}{s} \cdot \frac{k_T}{(J_L + J_M)} \tag{8}$$

While in the high frequency band, $s \to \infty$, the dominator is s^2, so $G_2(s) \approx k_T / J_M$ (4) can be simplified to (9), which is equivalent to the motor working without any load.

$$G''_{Plant}(s) = l_2(s) = \frac{k_T}{J_M \cdot s} \cdot \frac{1}{(T_f s + 1)^2} \tag{9}$$

However, the specific values of J_L and K_S are very difficult to get in the real practice. The usual method is to simplify the FRD model and identify the parameters. Table 1 shows the fitted parameters of the two-inertia model. It is important to stress that these fitted parameters are not realistic and of no physical significance, because of the simplification in the process.

It can be seen from Fig. 5 that the fitted transfer function $G_{Plant}(s)$ perfectly fits the real tested FRD model. Due to the existence of mechanical resonance, the amplitude-frequency characteristic of the system in the high frequency band is raised, thereby reducing the gain margin of the control system, and thus the bandwidth of the control system cannot be improved.

TABLE 1. Identified parameters for two-inertia model.

Symbol	Units	Values
k_T	$N \cdot m/A$	794.385
J_M	$Kg \cdot m^2$	0.395
K_s	$N \cdot m/rad$	112871.38
J_L	$Kg \cdot m^2$	2.05
b_s	–	0.205

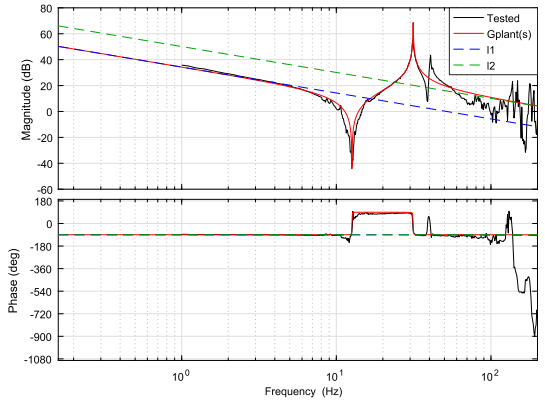

FIGURE 5. Bode diagram of two-inertia model and tested model.

III. ACTIVE DISTURBANCE REJECTION CONTROL FOR TWO-INERTIA MODEL

From the above discussion, we can see that if $G_2(s)$ can be compensated, $G_{Plant}(s)$ becomes an ideal rigid plant which is easy to control. ADRC is that kind of method that can treat $G_2(s)$ as disturbance, which can be estimated and compensated in real time [25]. Based on this theory, this section firstly presents the methodology of the framework and proposed controller, and then the stability of the closed loop control system is proved. Secondly, based on frequency domain analysis, the principles of suppressing mechanical resonance of LADRC and AFC are discussed. Finally, the comparison between ADRC and AFC is theoretically analyzed, and the advantages and disadvantages of ADRC are discussed.

A. PROPOSED METHOD FOR TELESCOPE

The control method proposed in this paper is shown in Fig. 6. This scheme consists of three elements: the position loop controller, the speed loop controller, and the NTD feedforward. The position loop controller is traditional PI controller. The speed loop controller is NADRC which consists of NESO and a proportional feedback control law. The NTD feedforward controller consists of an acceleration feedforward controller and a speed feedforward controller.

1) SPEED LOOP CONTROLLER DESIGN

The principle of the speed loop NADRC is shown in Fig. 6. Ignoring the T_f in (4), the transfer function from I_{ref} to θ_M is

$$G_{vplant}(s) = \frac{\theta_M}{I_{ref}} = G_{plant}(s) \cdot \frac{1}{s}$$

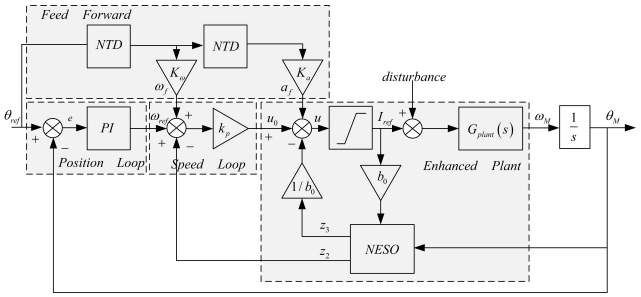

FIGURE 6. Block diagram of proposed method for telescope control system.

$$= \frac{k_T}{(J_M + J_L)} \cdot \frac{1}{s^2} \cdot \frac{J_L s^2 + b_s s + K_s}{\frac{J_M J_L}{(J_M + J_L)} s^2 + b_s s + K_s} \quad (10)$$

Considering the external disturbance w, (10) can be rewritten as

$$J_M J_L \dddot{\theta}_M + b_s (J_M + J_L) \ddot{\theta}_M + K_s \ddot{\theta}_M = k_T \left(J_L \ddot{I}_{ref} + b_s \dot{I}_{ref} + K_s I_{ref} \right) + w \quad (11)$$

Integrating (11) twice on both sides, the fourth-order system with a relative degree of two becomes a second-order system as below

$$\ddot{\theta}_M = b_0 \cdot I_{ref} + f \quad (12)$$

where

$$b_0 = \frac{k_T}{J_M} \quad (13)$$

$$f = \frac{k_T b_s}{J_M J_L} \int I_{ref} + \frac{k_T K_s}{J_M J_L} \iint I_{ref} - \frac{b_s (J_M + J_L)}{J_M J_L} \theta_M - \frac{K_s (J_M + J_L)}{J_M J_L} \int \theta_M + \iint w \quad (14)$$

Here f, including both external disturbance and the resonance, represents the " total disturbance" to be estimated and compensated. Based on (12), it is better to choose a third-order ESO [22]. With x_1 and x_2 denoting θ_M and ω_M, and x_3 denoting f, (12) can be rewritten as

$$\begin{bmatrix} \dot{x}_1 \\ \dot{x}_2 \\ \dot{x}_3 \end{bmatrix} = \begin{bmatrix} 0 & 1 & 0 \\ 0 & 0 & 1 \\ 0 & 0 & 0 \end{bmatrix} \begin{bmatrix} x_1 \\ x_2 \\ x_3 \end{bmatrix} + \begin{bmatrix} 0 \\ b_0 \\ 0 \end{bmatrix} u + \begin{bmatrix} 0 \\ 0 \\ 1 \end{bmatrix} \dot{f}$$
$$y = \begin{bmatrix} 1 & 0 & 0 \end{bmatrix} \begin{bmatrix} x_1 \\ x_2 \\ x_3 \end{bmatrix} \quad (15)$$

So the corresponding NADRC control law is constructed as

$$ESO: \begin{cases} \varepsilon_1 = z_1 - \theta_M \\ \dot{z}_1 = z_2 - \beta_{01} \cdot \varepsilon_1 \\ \dot{z}_2 = z_3 - \beta_{02} \cdot fal\left(\varepsilon_1, \frac{1}{2}, \delta\right) + \hat{b}_0 I_{ref} \\ \dot{z}_3 = -\beta_{03} \cdot fal\left(\varepsilon_1, \frac{1}{4}, \delta\right) \end{cases} \quad (16)$$

$$fal(\varepsilon_1, a, \delta) = \begin{cases} \dfrac{\varepsilon_1}{\delta^{(1-a)}} & |\varepsilon_1| \leqslant \delta \\ sign(\varepsilon_1)\,|\varepsilon_1|^a & |\varepsilon_1| > \delta \end{cases} \tag{17}$$

$$u_0 = k_p\left(\omega_{ref} - z_2\right) \tag{18}$$

$$u = u_0 - \frac{z_3}{\hat{b}_0} \tag{19}$$

According to [26], the anti-windup of NADRC is designed as

$$I_{ref} = \begin{cases} I_{\min} & u < I_{\min} \\ u & I_{\min} < u < I_{\max} \\ I_{\max} & u > I_{\max} \end{cases} \tag{20}$$

where θ_{ref} is the reference position, ω_{ref} is the reference speed, u_0 is the virtual control signal, u is the compensated control signal, I_{ref} is the actual control signal, ε_1 is the observer error, β_{01}, β_{02} and β_{03} are observer gains, $\hat{b}_0$ is the estimated value of b_0, δ is the parameter to be tuned, k_p is the controller gain. z_1 and z_2 are observer states tracking θ_M and ω_M respectively, here z_3 is the extended state which is the estimation of f in real time. Assuming that the controller is unsaturated, so

$$I_{ref} = u = u_0 - \frac{z_3}{\hat{b}_0} \tag{21}$$

Substituting (21) into (12),

$$\ddot{\theta}_M = b_0 \cdot u_0 - b_0 \cdot \frac{z_3}{\hat{b}_0} + f \tag{22}$$

With $\hat{b}_0 \approx b_0$ and $z_3 \approx f$, we have

$$\begin{cases} \ddot{\theta}_M \approx b_0 \cdot u_0 \\ \dot{\omega}_M \approx b_0 \cdot u_0 \end{cases} \tag{23}$$

It can be seen from (23) that the total disturbance is ''cancelled'' and the plant of speed becomes an ideal rigid plant, so the ideal closed-loop control of speed can be achieved by a simple proportional controller in (18).

2) POSITIOIN LOOP CONTROLLER DESIGN

The position loop controller in Fig. 6 is a traditional PI controller

$$G_{PI}(s) = k_p' + k_i' \cdot \frac{1}{s} \tag{24}$$

k_p' is the proportional gain, k_i' is integral coefficient.

3) FEEDFORWARD CONTROLLER DESIGN

In order to improve the accuracy of the control system, the feedforward control is used. The differential du/dt calculation can be not realized in reality. So the widely used feedforward method is shown in (25), the differential result is filtered by a first-order or second-order low-pass filter, is the time constant of the low-pass filter, however these methods are either too noisy or have large phase lag.

$$G_D(s) = \frac{s}{T_D s + 1} or \frac{s}{(T_D s + 1)^2} \tag{25}$$

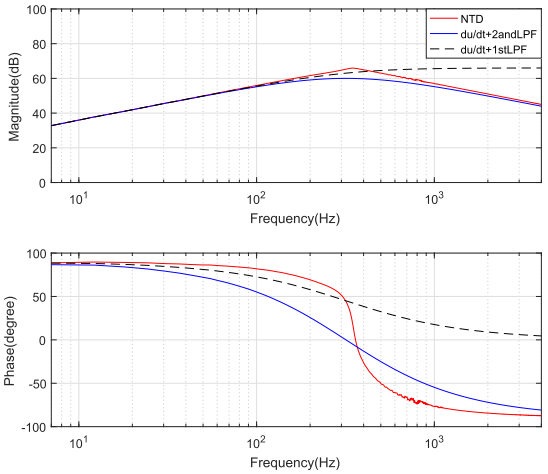

FIGURE 7. Bode diagram of NTD and du/dt + LPF ($h = 0.00001$, $h_0 = 10h$, $T_D = 0.0005$, $r = 0.8772/T_D^2$).

In this paper, NTD is used to solve these problems [27], as shown in (25)(26).

$$\begin{cases} fh = fhan\left(\tilde{x}_1(k) - v(k), \tilde{x}_2(k), r, h_0\right) \\ \tilde{x}_1(k+1) = \tilde{x}_1(k) + h\tilde{x}_2(k) \\ \tilde{x}_2(k+1) = \tilde{x}_2(k) + h \cdot fh \end{cases} \tag{26}$$

$$\begin{cases} d = rh_0 \\ d_0 = h_0 d \\ y_1 = (\tilde{x}_1(k) - v(k)) + h_0\tilde{x}_2(k) \\ a_0 = \sqrt{d^2 + 8r|y|} \\ a_1 = \begin{cases} \tilde{x}_2(k) + \dfrac{(a_0 - d)}{2} sign(y), & |y_1| > d_0 \\ \tilde{x}_2(k) + \dfrac{y}{h_0}, & |y_1| \leqslant d_0 \end{cases} \\ fhan = -\begin{cases} rsign(a_1), & |a_1| > d \\ r\dfrac{a_1}{d}, & |a_1| \leqslant d \end{cases} \end{cases} \tag{27}$$

where $v(k)$ is the reference input, $\tilde{x}_1(k)$ is the state tracking $v(k)$, $\tilde{x}_2(k)$ is the differential of $\tilde{x}_1(k)$, h is the sampling interval, h_0, d, d_0, y_1, a_0 and a_1 are the intermediate variables, r the speed factor which determines the tracking speed to be tuned.According to [28], the relationship between r and the bandwidth ω_{TD} is

$$\omega_{TD} = 1.14\sqrt{r} \tag{28}$$

By sine sweep measurement method, the Bode diagram of (24) and $\tilde{x}_2$ in (27) is obtained. As shown in, the three methods have the same bandwidth of 318 Hz. It can be seen that the phase angle of NTD basically maintains about 90^0 ahead inside of bandwidth, whereas outside of bandwidth the phase angle is rapidly down to -90^0, which shows that NTD is an ideal differentiator.

Therefore, speed and acceleration feedforward controllers can be designed as NTD:

$$\begin{cases} \theta_{ref\_f}(k+1) \\ = \theta_{ref\_f}(k) + h\omega_f(k) \\ \omega_f(k+1) \\ = \omega_f(k) + hfhan\left(\theta_{ref\_f}(k) - \theta_{ref}(k), \omega_f(k), r, h_0\right) \\ \omega_{ref\_f}(k+1) \\ = \omega_{ref\_f}(k) + ha_f(k) \\ a_f(k+1) \\ = a_f(k) + hfhan\left(\omega_{ref\_f}(k) - \omega_{ref}(k), a_f(k), r, h_0\right) \end{cases} \tag{29}$$

$\theta_{ref}(k)$ is the position reference signal, $\theta_{ref\_f}(k)$ is the state tracking $\theta_{ref}(k)$, $\omega_f(k)$ is feedforward speed, $\omega_{ref\_f}(k)$ is the state tracking $\omega_f(k)$, $a_f(k)$ is feedforward acceleration, K_ω and K_a are parameters to be tuned.

4) THE FINAL CONTROLLER

Based on the above design, the control algorithm proposed in this paper can be divided into three parts: 1) The first part is NESO, as shown in (16). 2) The second part is the feedforward part, which consists of two NTDs in series, as shown in (29). 3) The third part is speed loop controller and position loop PI controller. Ignoring the saturation effect, (18)(19)(21) (24) can be written as

$$\begin{aligned} ADRC: I_{ref} &= k_p k'_p\left(\theta_{ref} - \theta_M\right) \\ &+ k_p k'_i \int \left(\theta_{ref} - \theta_M\right)dt + k_p K_\omega \omega_f \\ &+ K_a a_f - k_p z_2 - \frac{z_3}{\hat{b}_0} \end{aligned} \tag{30}$$

5) STABILITY ANALYSIS

The stability proof of NADRC is very difficult, and keeps un-proved for decades. Up until recent years the problem was solved, the rigorous convergence proofs of the NESO and the NTD were conducted in [29], [30], and the stability of traditional NADRC in [22] for SISO system was proved in [31]. Theorem 5 in [31] indicates that the system is stable if Assumptions A1-A4 are satisfied. Theorem 5 and Assumptions A1-A4 are shown in the Appendix A. This paper mainly focuses on the practical application, so only the improved parts in this paper will be proved and some existing conclusions in the literatures will be used.

Assumption 1 is made for the boundedness of the system itself and the external disturbance. For general practical systems, Assumption 1 holds. The convergence of ESO and TD used in this paper are proved in [29] and [30], so Assumption 2 and A4 hold. Therefore, here we only need to prove that (30) satisfies Assumption 3, and Assumption 3 in [31] is described as follows

Assumption 3 $\varphi(v)$ is continuously differentiable, $\varphi(0) = 0$, and Lipschitz continuous with Lipschitz constant L:$\left|\varphi(v) - \varphi\left(\hat{v}\right)\right| \leqslant L\left\|v - \hat{v}\right\|$for all $v, \hat{v} \in \mathbb{R}^n$.There exist constants $\lambda_{2i}(i = 1, 2, 3, 4)$, β_2, and positive continuous differentiable function V_2, W_2:$\mathbb{R}^{n+1} \to \mathbb{R}$ such that

$$\lambda_{21}\|v\|^2 \leqslant V_2(v) \leqslant \lambda_{22}\|v\|^2, \lambda_{23}\|v\|^2 \leqslant W_2(v) \leqslant \lambda_{24}\|v\|^2 \tag{31}$$

$$\sum_{i=1}^{n-1} v_{i+1}\frac{\partial V_2(v)}{\partial v_i} + \varphi(v_1, v_2, \ldots, v_n)\frac{\partial V_2(v)}{\partial v_n} \leqslant -W_2(v) \tag{32}$$

$$\left|\frac{\partial V_2(v)}{\partial v_n}\right| \leqslant \beta_2\|v\|, \quad \forall v = (v_1, v_2, \ldots, v_n) \in \mathbb{R}^n \tag{33}$$

Let $K_\omega = 1$, $K_a = 1/\hat{b}_0$, (30) can be rewritten as

$$\begin{aligned} I_{ref} &= \frac{1}{\hat{b}_0}\left(-\hat{b}_0 k_p k'_i \int \left(\theta_M - \theta_{ref}\right)dt\right) \\ &+ \left(-\hat{b}_0 k_p k'_p\left(\theta_M - \theta_{ref}\right)\right) \\ &+ \left(-\hat{b}_0 k_p\left(z_2 - \omega_f\right) + a_f - z_3\right) \end{aligned} \tag{34}$$

We can see from (30) that the controller of proposed method is linear, and the corresponding $\varphi(\cdot)$ in Assumption 3 is

$$\varphi(x_1, x_2, x_3) = -\hat{b}_0 k_p k'_i x_1 - \hat{b}_0 k_p k'_p x_2 - \hat{b}_0 k_p x_3 \tag{35}$$

Apparently $\varphi(x_1, x_2, x_3)$ is Lipschitz continuous.
Let

$$A = \begin{bmatrix} 0 & 1 & 0 \\ 0 & 0 & 1 \\ -\hat{b}_0 k_p k'_i & -\hat{b}_0 k_p k'_p & -\hat{b}_0 k_p \end{bmatrix} \tag{36}$$

With appropriate parameters, A can be Hurwitz.
Let

$$V(x) = \langle P_A x, x\rangle \tag{37}$$

$$W(x) = \|x\|^2 = x_1^2 + x_2^2 + x_3^2 \tag{38}$$

Here $\forall x = (x_1, x_2, x_3)^T \in \mathbb{R}^n$, P_A is the positive definite matrix that is the unique solution of the Lyapunov equation $P_A A + A^T P_A = -I_n$, I_n is a 3-dimensional identity matrix.
Then

$$\lambda_{21}\|x\|^2 \leqslant V(x) \leqslant \lambda_{23}\|x\|^2 \tag{39}$$

$$\begin{aligned} &\sum_{i=1}^{n-1} x_{i+1}\frac{\partial V}{\partial x_i} - \left(\hat{b}_0 k_p k'_i x_1 + \hat{b}_0 k_p k'_p x_2 + \hat{b}_0 k_p x_3\right)\frac{\partial V}{\partial x_n} \\ &= -\langle x, x\rangle = -W(x) \end{aligned} \tag{40}$$

And

$$\left|\frac{\partial V}{\partial x_n}\right| \leqslant \beta_2(P_A)\|x\| \tag{41}$$

Therefore, $V(x)$ and $W(x)$ satisfy the conditions of Assumption 3.

So the Assumptions A1-A4 are all satisfied, and the proposed method is stable. A numerical analysis is presented in the Appendix B.

B. THE PRINCIPLE OF ADRC AND AFC SUPPRESSING MECHNIACL RESONANCE

1) THE PRINCIPLE OF ADRC SUPPRESSING MECHNIACL RESONANCE

The ESO is the core of ADRC, which improves the control performance through observing and compensating the internal and external disturbances. This section focuses on the principle of ESO suppressing mechanical resonance. Fig.8 shows the disturbance observing and compensating part of the ESO. Since the NESO cannot be analyzed by transfer function, a linearized ESO is used here for analysis. And in order to simplify the discussion, it is assumed that there is a speed sensor in the system, so a second-order ESO will be used. All parts f_0 that corrupt the ideal integral component are regarded as ''disturbance''. If the estimated disturbance $\tilde{z}_2$ of ESO rapidly converges to f_0,then the disturbance encountered by the ideal plant can be well compensated.

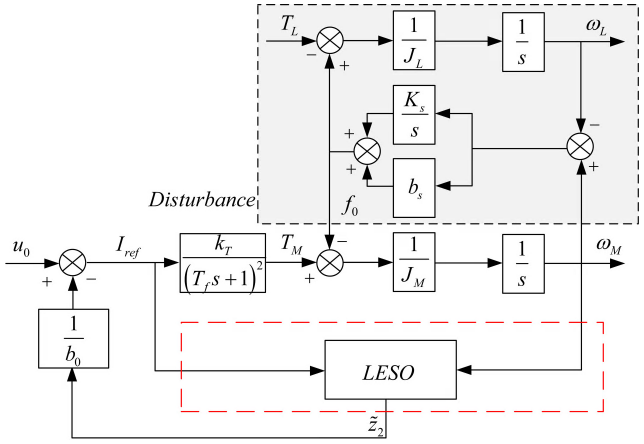

FIGURE 8. Block diagram LESO.

According to the above assumptions, and ignoring T_f and saturation in Fig. 8, (4) can be written as follows

$$\dot{\omega}_M = b_0 \cdot I_{ref} + f_0 \tag{42}$$

where

$$f_0 = \frac{k_T b_s}{J_M J_L}\int I_{ref} + \frac{k_T K_s}{J_M J_L}\iint I_{ref} - \frac{b_s (J_M + J_L)}{J_M J_L}\omega_M - \frac{K_s (J_M + J_L)}{J_M J_L}\int \omega_M + \iint w \tag{43}$$

Then the corresponding second-order LESO is

$$\begin{cases} \tilde{\varepsilon}_1 = \tilde{z}_1 - \omega_M \\ \dot{\tilde{z}}_1 = \dot{\tilde{z}}_2 - \tilde{\beta}_{01} \cdot \tilde{\varepsilon}_1 + \hat{b}_0 I_{ref} \\ \dot{\tilde{z}}_2 = -\tilde{\beta}_{02} \cdot \tilde{\varepsilon}_1 \end{cases} \tag{44}$$

Here, $\tilde{z}_1$ and $\tilde{z}_2$ are observer states tracking ω_M and f_0, $\tilde{\beta}_{01}$ and $\tilde{\beta}_{02}$ are observer gains. Using the parameterization technique proposed in [32], let $\begin{bmatrix} \tilde{\beta}_{01} & \tilde{\beta}_{02} \end{bmatrix}^T = \begin{bmatrix} 2\omega_o & \omega_o^2 \end{bmatrix}^T$, ω_o is the observer bandwidth. By Laplace transformation, the disturbance observed is

$$\tilde{Z}_2(s) = \frac{-b_0\omega_o^2}{(s+\omega_o)^2} \cdot I_{ref}(s) + \frac{\omega_o^2 s}{(s+\omega_o)^2} \cdot \Omega_M(s) \tag{45}$$

If $T_f = 0$, combining (4) and (45), using the Masonąŕs gain formula (MGF), the transfer function of the enhanced plant can be expressed as

$$G_{LESO}(s) = \frac{\omega_M}{u_0} = \frac{k_T}{J_M + \left(1 - \frac{\omega_o^2}{(s+\omega_o)^2}\right) \cdot J_L} \cdot \frac{J_L \cdot s^2 + b_s \cdot s + K_s}{\frac{J_M}{J_M + \left(1 - \frac{\omega_o^2}{(s+\omega_o)^2}\right) \cdot J_L} \cdot J_L \cdot s^2 + b_s \cdot s + K_s} \cdot \frac{1}{s} \tag{46}$$

Let

$$f_{LESO}(s) = \frac{J_M}{J_M + \left(1 - \frac{\omega_o^2}{(s+\omega_o)^2}\right) \cdot J_L} \tag{47}$$

Within the observer bandwidth of ω_o, we can get $\omega_o^2/(s+\omega_o)^2 = 1$, so $f_{LESO}(s) = 1$, Then equation (46) can be simplified to

$$G_{LESO}(s) = \frac{k_T}{J_M} \cdot \frac{1}{s} \tag{48}$$

$G_{LESO}(s)$ is an ideal plant. Therefore, as long as the observer bandwidth of the ESO satisfies $\omega_o > \omega_N$,the mechanical resonance of the system can be well suppressed, and the system becomes an ideal plant. Fig. 9 shows the Bode diagram of $G_{LESO}(s)$ under different observer bandwidth. It indicates that the ADRC method can effectively suppress mechanical resonance. The larger the observer bandwidth is, the closer the plant is to $l_2(s)$, and the better the suppress effect.

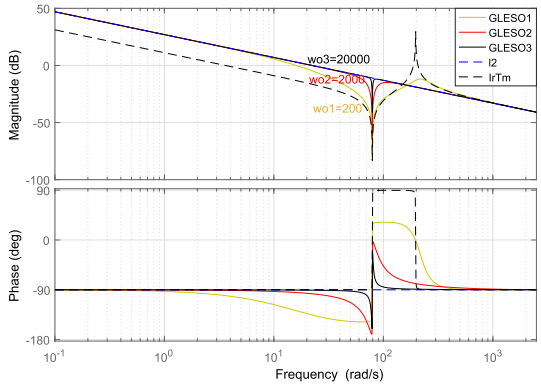

FIGURE 9. Bode diagram enhanced plant (from u_0 to ω_M), the parameters are shown in the Table 1 and the observer bandwidth are ω_o, $10\omega_o$, $100\omega_o$ ($\omega_o = 200$).

We can see from Fig. 9 that the principle of ADRC suppressing the mechanical resonance is reducing the load inertia as close as possible to zero by electronic means, thus reducing the coupling between the motor and the load. In this scenario,

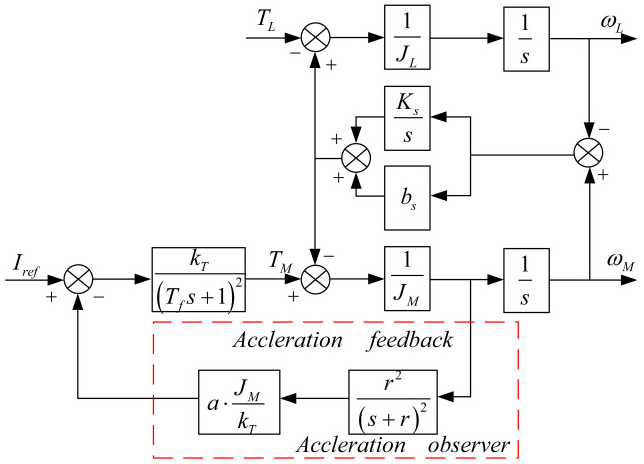

FIGURE 10. Block diagram of ideal acceleration feedback.

the motor can work as equivalent to no load in the low frequency band, and effectively suppressing the mechanical resonance. Theoretically, if we want to construct the enhanced plant to a pure integral component through ESO, the observer bandwidth ω_o needs to be infinite.

2) THE PRINCIPLE OF AFC SUPPRESSING MECHNIACL RESONANCE

In order to demonstrate the resonance suppressing performance of ADRC, in this section the AFC method is simply discussed.

As shown in Fig. 10, assuming that the transfer function of the ideal acceleration observer is $G_{as}(s) = r_o{}^2/(s+r_o)^2$, r_o is the observer bandwidth of the acceleration observer, feedback gain is a, and $T_f \approx 0$. The estimated acceleration is feed back to the current loop. Using the MGF, we can get

$$G_{AFC}(s) = \frac{\omega_M}{I_{ref}} = \frac{k_T}{\left(1+\frac{a\cdot r_o{}^2}{(s+r_o)^2}\right)\cdot J_M + J_L} \times \frac{J_L\cdot s^2 + b_s\cdot s + K_s}{\frac{\left(1+\frac{a\cdot r_o{}^2}{(s+r_o)^2}\right)\cdot J_M}{\left(1+\frac{a\cdot r_o{}^2}{(s+r_o)^2}\right)\cdot J_M + J_L}\cdot J_L\cdot s^2 + b_s\cdot s + K_s} \times \frac{1}{s} \tag{49}$$

Let

$$f_{AFC}(s) = \frac{\left(1+\frac{a\cdot r_o{}^2}{(s+r_o)^2}\right)\cdot J_M}{\left(1+\frac{a\cdot r_o{}^2}{(s+r_o)^2}\right)\cdot J_M + J_L} \tag{50}$$

The principle of AFC for suppressing the mechanical resonance is raising the inertia of the motor by electronic means, effectively reduces the amplitude of the transfer function in the high frequency band, thereby suppressing the mechanical resonance. Theoretically, if we want to change the plant to an ideal pure integral by AFC, the observer bandwidth r_o needs to be infinite and the value of a needs to be large enough.

C. COMPARISON OF THE TWO METHODS

According to the above analysis, we can see that the two methods both want to enhance the original plant show in (4) to an ideal pure integral component, so that the mechanical resonance is suppressed. Here is a comparison of the advantages and disadvantages of the two methods.

Given the same observer bandwidth $r_o = \omega_o > \omega_N$, the Bode diagrams of $f_{LESO}(s)$ and $f_{AFC}(s)$ are shown in Fig. 11. When $\omega_N < \omega_{cross}$, ω_{cross} is the intersection point of $f_{LESO}(s)$ and $f_{AFC}(s)$, $f_{LESO}(s)$ is closer to 1 than $f_{AFC}(s)$, so $G_{LESO}(s)$ is closer to the ideal plant than $G_{AFC}(s)$, and the larger the feedback gain, the better the effect as can be seen in Fig. 12.

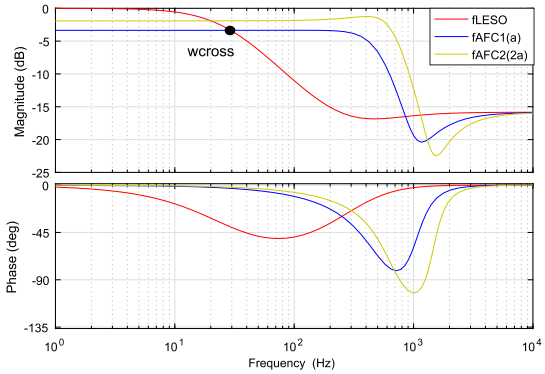

FIGURE 11. Bode diagram of $f_{LESO}(s)$ and $f_{AFC}(s)$, the parameters are shown in the Table 1 and $r_o = \omega_o = 2000$, $a = 10$, $2a = 20$.

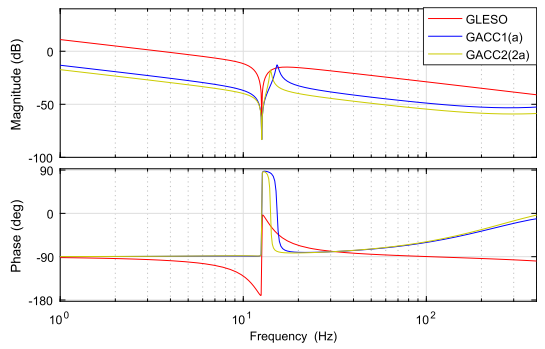

FIGURE 12. Bode diagram of $G_{LESO}(s)$ and $G_{AFC}(s)$, the parameters are shown in the Table 1 and $r_o = \omega_o = 2000$, $a = 10$, $2a = 20$.

As shown in Fig. 13, when $r_o = \omega_o = 2000$ and load inertia J_L increases from J_L to $10J_L$, the magnitude of $f_{AFC2}(s)$ decrease, thus the performance of AFC decreases. Fig. 14 indicates that LESO still has very good effects. The feedback gain a of AFC needs to be tuned larger to obtain an effect similar to LESO. From the above discussion, we can conclude that for low-frequency mechanical resonance, ESO is better; whereas for higher mechanical resonance, AFC is better.

As shown in Fig. 15, the ESO improves the open loop gain at the low frequency and reduces the open loop gain at the high frequency, thus a simple proportional controller

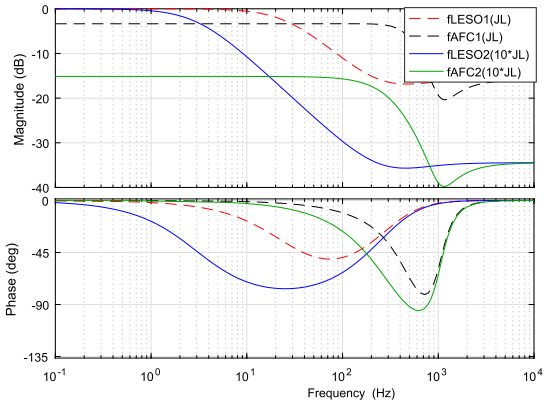

FIGURE 13. Bode diagram of $f_{LESO}(s)$ and $f_{AFC}(s)$, the parameters are shown in the Table 1 and $r_o = \omega_o = 2000$, $a = 10$.

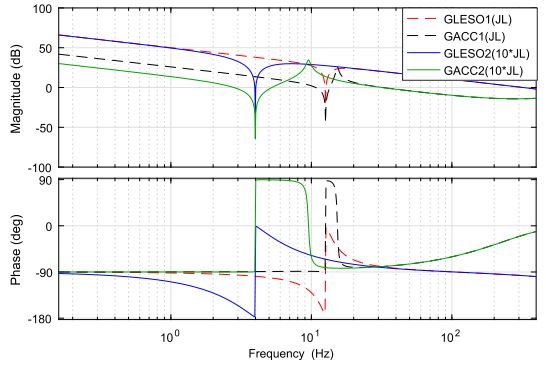

FIGURE 14. Bode diagram of $G_{LESO}(s)$ and $G_{AFC}(s)$, the parameters are shown in the Table 1 and $r_o = \omega_o = 2000$, $a = 10$.

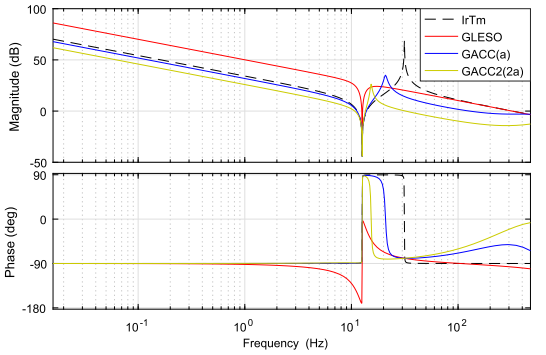

FIGURE 15. Bode diagram of LESO and AFC (from I_{ref} to ω_M), the parameters are shown in the Table 1 $r_o = \omega_o = 2000$, $a = 10$.

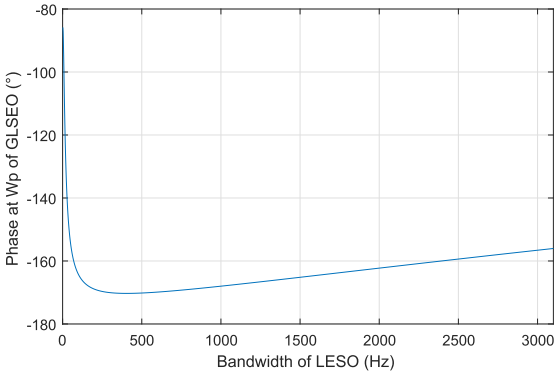

FIGURE 16. Phase of GLESO at ω_A when the bandwidth of the LESO changing.

can satisfy the requirements. However, ESO also has its disadvantage: ESO suppressing the resonant frequency at the cost of reducing the phase margin. Fig. 16 shows the phase margin of the enhanced plant under different observer bandwidths. When ω_o is less than 318 Hz, the phase angle of the system becomes smaller as the ω_o increases. When the ω_o is greater than 318 Hz, the phase angle of the system increases with the increase of ω_o. In practical, the bandwidth of ESO should not be too low, because ESO with low bandwidth has limited effect; nor can it be too high, such that the noise will be amplified. Therefore, ADRC is good at suppressing the low frequency mechanical resonance. For higher frequency mechanical resonance, the bandwidth of ESO needs to be very high which is not realizable in actual application. Fortunately, NESO has much better observing efficiency than LESO which may relief the phase loss [28]. And in the application scenario of large telescopes, the mechanical resonant frequency is very low, and the noise of the system has already been effectively reduced, so the bandwidth of the ESO can be appropriately increased.

IV. EXPERIMENT

The experiment setup is shown in Fig. 17. It consists of an operating console, a telescope control unit, a servo controller, and a large telescope. The measured FRD model of azimuth axis of the telescope is shown in Fig. 2. The telescope control unit is an embedded computer with real-time operating system. The servo controller can control and drive both azimuth and elevation axes at the same time. The MCU of servo controller is TMS320F28335, and the IPM modules are Mitsubishi PM200CLA120. The angular measuring system is consist of a Renishaw grating ruler and two read heads, and the grating ruler has 86400 pulses and the read head is 400 times subdivision. It can be calculated that one pulse represents 0.009375 arc-second (including a four-fold increase in resolution by the quadrature encoder pulse (QEP) module). is the friction torque of the shaft. The current sampling frequency is 8 kHz, and the encoder sampling frequency is 2 kHz. Since the control systems of azimuth and elevation axes have the same architecture, the azimuth axis is used for comparison and verification. The acceleration observer used here is Luenberger observer described in [5], and the parameters are: $a = 25$, $k_{ap} = 365$, $k_{ai} = 150$, $k_{ad} = 179$. The speed and position controller of AFC method are PI controllers in series, the speed parameters are: $k_{sp} = 0.3$, $k_{si} = 0.07$, the position parameters are: $k_{pp} = 11.7$, $k_{pi} = 2.29$.

The tuning of the proposed control strategy is as follows:

1) The first step is to determine the parameters of LADRC in the speed loop. According to Table 1,

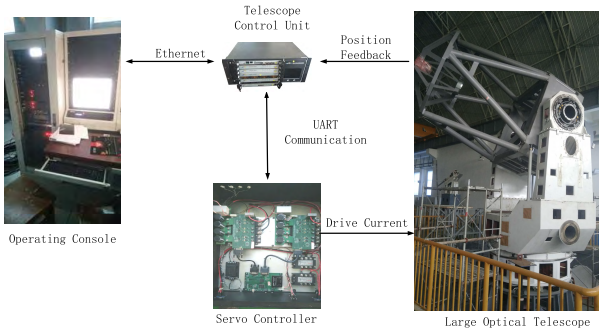

FIGURE 17. Experimental setup.

TABLE 2. Main parameters used in the experiment.

Symbol	Units	Values
k_T	$N \cdot m/A$	8.8
T_F	$N \cdot m$	25
ω_o	Hz	318
$\hat{b}_0$	–	2011
δ	–	0.05
k_p	–	0.014
k'_p	–	11.7
k'_i	–	2.29
r	–	798.5
h_0	–	0.005
K_ω	–	1
K_a	–	0.005
a	–	25
k_{ap}	–	365
k_{ai}	–	150
k_{ad}	–	179
k_{sp}	–	0.3
k_{si}	–	0.07
k_{pp}	–	11.7
k_{pi}	–	2.29

$\hat{b}_0 = k_T/J_M \approx 2011$. The observer bandwidth ω_o and the controller gain k_p can be tuned by according to the bandwidth method [32].

2) The second step is to determine the parameters of NADRC. According to the typical third-order NESO empirical formula in [33]: $\delta = 0.05$, $\beta_{01} = 3\omega_o$, $\beta_{02} = 3\omega_o^2/5$, $\beta_{03} = \omega_o^3/9$, so the parameters of NESO are determined. And the controller gain of NADRC can be selected as k_p in step one.

3) The parameters k'_p, k'_i of PI in the position loop can be tuned by using Ziegler-Nichols tuning rules.

4) In the feedforward NTD: h_0 is determined by $h_0 = 10h = 0.005$ [28](in this experiment $h = 0.0005$), can be selected by the bandwidth method in (27). The feedforward gains K_ω can be set to 1, and K_a can be set to $1/b_0 \approx 0.0005$ [34].

From above discussion, It can be concluded that the proposed controller only has 5 parameters to tune: ω_o, k_p, r, k'_p and k'_i. The parameters used in the experiment are listed in the Table 2.

As shown in Fig. 18, both the AFC and the ADRC enhance the plant to a relative ideal plant. Unlike above analyses based on the simplified two-inertia model, the AFC method also has a large phase loss at the anti-resonant frequency

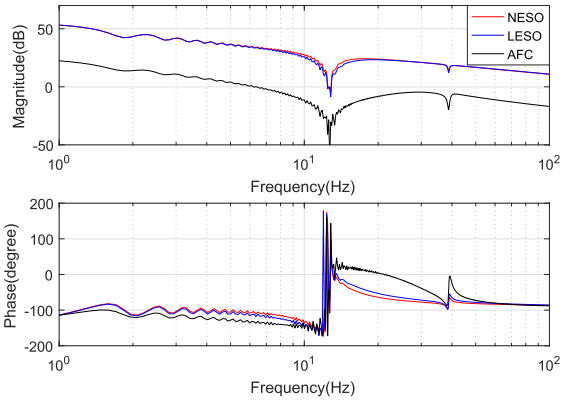

FIGURE 18. Enhanced plant comparison (from u_0 to ω_M).

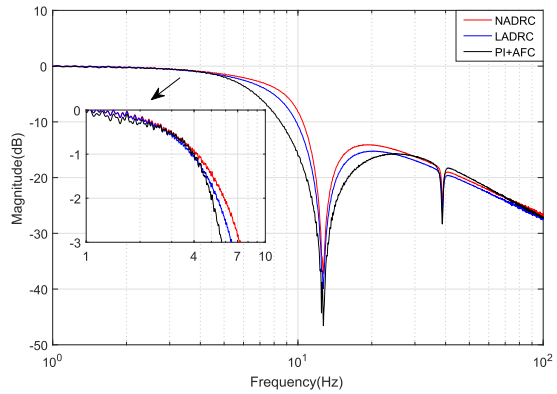

FIGURE 19. Speed close-loop Bode comparison (from ω_{ref} to ω_M).

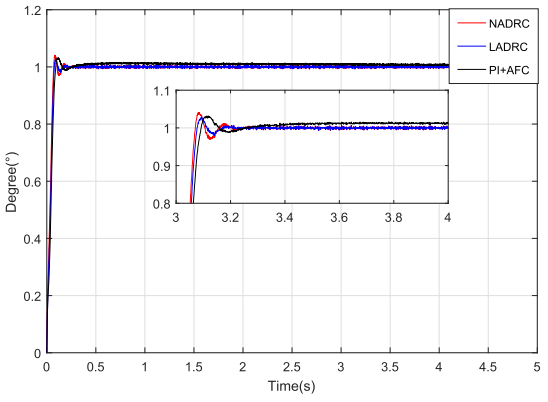

FIGURE 20. Speed step comparison.

for multi-inertia systems. What's more, the phase angle of NADRC is bigger than LADRC, and much bigger than AFC, which may give better robustness. In Fig. 19, the bandwidth of the speed loop is higher than AFC by using NADRC. The step response in Fig. 20 also demonstrates that NADRC is faster than the other methods.

The sensitivity Bode diagram of the position loop is shown in Fig. 21. The proposed composite control method still keeps the same error sensitivity peak as the other methods, and the position error sensitivity attenuation is strengthened in

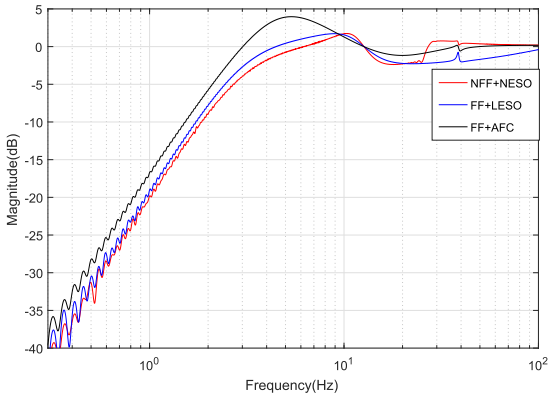

FIGURE 21. Position error sensitivity comparison (from θ_{ref} to θ_{err}).

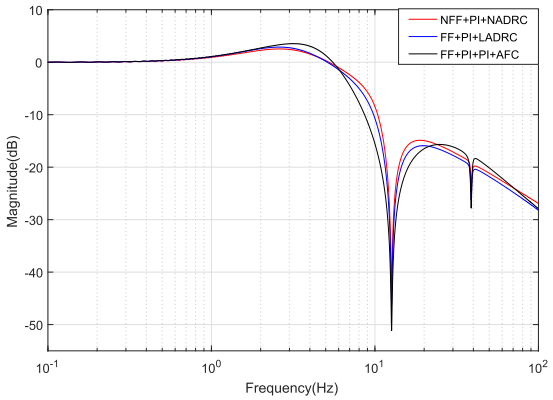

FIGURE 22. Position close-loop bode comparison (from θ_{ref} to θ_M).

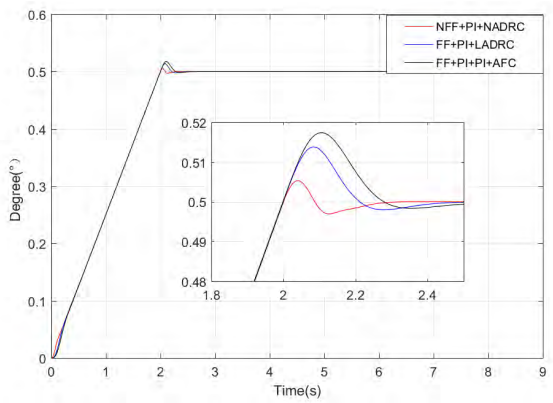

FIGURE 23. Position trapezoidal wave tracking comparison.

low frequency range and boosted slightly in higher frequency range where the disturbance is small in telescope control system. By this way, the tracking accuracy is improved. Fig. 22 is closed-loop Bode diagram of position loop, it can be seen that the resonance peak of the proposed method is the smallest. The presence of a resonant peak will cause position overshoot, whereas, for telescope, the reference signal is often a low-frequency sinusoidal like signals. Fig. 23 shows the trapezoidal wave tracking curve of the telescope. The

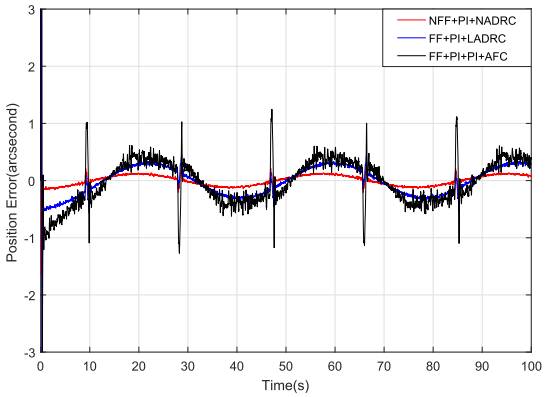

FIGURE 24. Position error of sinewave tracking.

TABLE 3. Position error comparison.

θ_{ref}	FF+PI+PI+AFC		FF+PI+LADRC		FF+PI+NADRC	
	PV	RMS	PV	RMS	PV	RMS
$y = 36^0 \sin(0.17t)$	2.51	0.95	1.12	0.67	0.59	0.18
$y = 50^0 \sin(0.2t)$	2.15	1.61	1.31	1.14	0.53	0.31
$y = 36^0 \sin(0.33t)$	4.46	2.27	2.76	1.56	0.71	0.38
$y = 32^0 \sin(0.5t)$	9.15	3.94	4.53	2.56	1.12	0.56

PV stands for peak to peak value, RMS stands for root mean square. The unit is arc-second.

proposed method has the smallest overshoot and the fastest convergence. Fig. 24 shows the tracking error curve of the sine wave $y = 36^0 \sin(0.1667t)$.

Table 3 shows the different sinusoidal tracking errors. The error is reduced by using the method proposed, and the proposed method also has a good suppression effect on some nonlinear and unknown disturbances such as friction, dead zone and noise.

V. CONCLUSION

This paper studies the use of the ADRC technique to suppress the multi low mechanical resonances appearing in the large optical telescope. First, a simplified physical model was established. Concerned about the control of the motor position, a third-order NESO was designed to estimate and compensate the original plant to an ideal rigid plant, which decouples the compliance between the motor and the load. Moreover, a PI controller was used to achieve a high precision position tracking of the telescope. Then based on the NTD, a speed and acceleration feedforward is established such that the tracking performance can be improved. The principle of suppression mechanical resonance of ESO is analyzed in frequency domain. Comparing with AFC, it can be concluded that the ADRC is better than AFC at suppressing the low frequency mechanical resonance, whereas for higher frequency mechanical resonance, AFC is better. As confirmed by the experimental results, the proposed control system has good low-frequency mechanical resonances suppressing effect, command-following performance and is robust against all kinds of disturbances.

APPENDIX A
ASSUMPTIONS AND THEORME

This section describes the main conclusions of [31]. For an n-dimensional SISO nonlinear system which can be written as

$$\begin{cases} \dot{\widehat{x}}_1(t) = \widehat{x}_2(t) \\ \dot{\widehat{x}}_2(t) = \widehat{x}_3(t) \\ \quad \vdots \\ \dot{\widehat{x}}_n(t) = \widehat{f}\left(t, \widehat{x}_1(t), \ldots, \widehat{x}_n(t), \widehat{w}(t)\right) + b\widehat{u}(t) \\ \widehat{y}(t) = \widehat{x}_1(t) \end{cases} \tag{51}$$

where $\widehat{y}(t)$ is the output, $\widehat{u}(t)$ is the input, $\widehat{w} \in C^1([0,\infty), \mathbb{R})$ is the external disturbance, $\widehat{f} \in C^1\left(\mathbb{R}^{n+2}, \mathbb{R}\right)$ represents the nonlinear function of the plant which is possibly unknown, and $\widehat{b} > 0$ is a constant control coefficient which is not exactly known, but we have the nominal value $\widehat{b}_0$ that is sufficiently closed to $\widehat{b}$.

The ESO for system (51) is

$$\begin{cases} \dot{\widehat{x}}_1^*(t) = \widehat{x}_2^*(t) + \xi^{n-1}(t)\, g_1\left(\widehat{\theta}(t)\right) \\ \dot{\widehat{x}}_2^*(t) = \widehat{x}_3^*(t) + \xi^{n-2}(t)\, g_2\left(\widehat{\theta}(t)\right) \\ \quad \vdots \\ \dot{\widehat{x}}_n^*(t) = \widehat{x}_{n+1}^*(t) + g_n\left(\widehat{\theta}(t)\right) + \widehat{b}_0\widehat{u}(t) \\ \dot{\widehat{x}}_{n+1}^*(t) = \dfrac{1}{\xi(t)} g_{n+1}\left(\widehat{\theta}(t)\right) \end{cases} \tag{52}$$

where $\widehat{\theta}(t) = \left(\widehat{y}(t) - \widehat{x}_1^*(t)\right) \Big/ \xi^n(t)$, $\widehat{y}^*(t) = \widehat{x}_1^*(t)$, $g_i \in C(\mathbb{R}, \mathbb{R})$,and $\xi \in C\left([0,\infty), \mathbb{R}^+\right)$ is the gain function to be chosen to satisfy $\xi(0) = 1, \dot{\xi}(t) = -a\xi(t), a > 0$ if $\xi(t) > \varepsilon$, and $\dot{\xi}(0) = 0$.

A reference system is given as

$$\begin{cases} \dot{x}_1^*(t) = x_2^*(t) \\ \dot{x}_2^*(t) = x_3^*(t) \\ \quad \vdots \\ \dot{x}_n^*(t) = \varphi\left(x_1^*(t), \ldots, x_n^*(t)\right), \varphi(0, \ldots, 0) = 0 \end{cases} \tag{53}$$

where $\varphi \in C(\mathbb{R}^n, \mathbb{R})$. The TD can be rewritten as

$$\begin{cases} \dot{z}_{1R}^*(t) = z_{2R}(t) \\ \quad \vdots \\ \dot{z}_{nR}^*(t) = z_{(n+1)R}(t) \\ \dot{z}_{(n+1)R}(t) \\ \quad = R^n \psi\left(z_{1R}(t) - \upsilon(t), \dfrac{z_{2R}(t)}{R}, \ldots, \dfrac{z_{(n+1)R}(t)}{R^n}\right) \\ \psi(0, 0, \ldots, 0) = 0 \end{cases} \tag{54}$$

where R is the tuning parameter and $\psi \in C\left(\mathbb{R}^{n+1}, \mathbb{R}\right)$. The control objective of ADRC is to make $x_i(t)$ converge to $z_{iR}(t)$ or $\upsilon^{(i-1)}(t)$ in the way of reference system state $x_i^*(t)$ converging to zero. The controller of ADRC is

$$u(t) = \frac{1}{b_0}\left[\varphi\left(\widehat{x}_1^*(t) - z_R(t)\right) + z_{(n+1)R}(t) - \widehat{x}_{n+1}^*(t)\right] \tag{55}$$

where $\left(\left(\widehat{x}_1^*(t), \widehat{x}_2^*(t), \ldots, \widehat{x}_n^*(t)\right), \widehat{x}_{n+1}^*(t)\right)$ is the solution of (52) and $\left(\left(z_{1R}(t), z_{2R}(t), \ldots, z_{nR}(t)\right), z_{(n+1)R}(t)\right)$ is the solution of (54). The Assumption 1 below is made for the original system in (51) itself and the external disturbance.

Assumption 1: Both $\widehat{w}$ and $\dot{\widehat{w}}$ are bounded on $\mathbb{R}$, there exist positive constants $\bar{C}_1$, $\bar{C}_2$ and a non-negative function $\varpi \in C(\mathbb{R})$ such that

$$\left|\frac{\partial \widehat{f}\left(t, \widehat{x}, \widehat{w}\right)}{\partial \widehat{x}_i}\right| \leqslant \bar{C}_1 + \varpi, \quad i = 1, 2, 3, \ldots n, \tag{56}$$

$$\left|\widehat{f}\left(t, 0, \widehat{w}\right)\right| \leqslant \bar{C}_1 + \varpi$$

$$\left|\frac{\partial \widehat{f}\left(t, \widehat{x}, \widehat{w}\right)}{\partial \widehat{w}_i}\right| + \left|\frac{\partial \widehat{f}\left(t, \widehat{x}, \widehat{w}\right)}{\partial t_i}\right| \leqslant \bar{C}_1 + \bar{C}_2\left\|\widehat{x}\right\| + \varpi \tag{57}$$

The Assumption 2 is for ESO (52) and the unknown parameter $\widehat{b}_0$.

Assumption 2: $|g_i(r)| \leqslant \Lambda_i |r|$ for some positive constants Λ_i for $i = 1, 2, \ldots, n+1$. There exist constants λ_{1j} $(j = 1, 2, 3, 4)$, β_1, and positive definite continuous differentiable function $V_1, W_1 : \mathbb{R}^{n+1} \to \mathbb{R}$ such that

$$\begin{aligned} \lambda_{11}\|v\|^2 \leqslant V_1(v) \leqslant \lambda_{12}\|v\|^2 \\ \lambda_{13}\|v\|^2 \leqslant W_1(v) \leqslant \lambda_{14}\|v\|^2 \\ \forall v \in \mathbb{R}^{n+1} \end{aligned} \tag{58}$$

$$\sum_{i=1}^{n}\left(v_{i+1} - g_i(v_1)\right)\frac{\partial V_1(v)}{\partial v_i} - g_{n+1}(v_1)\frac{\partial V_1(v)}{\partial v_{n+1}} \leqslant -W_1(v), \quad \forall v \in \mathbb{R}^{n+1} \tag{59}$$

$$\left|\frac{\partial V_1(v)}{\partial v_{n+1}}\right| \leqslant \beta_1\|v\|, \quad \forall v = (v_1, v_2, \ldots, v_{n+1}) \in \mathbb{R}^{n+1} \tag{60}$$

Moreover, the parameter b_0 satisfies $B \triangleq \left|\frac{b-b_0}{b_0}\right| \Lambda_{n+1} < \frac{\lambda_{13}}{\beta_1}$.

The Assumption 3 is for reference system (53).

Assumption 3: $\varphi(v)$ is continuously differentiable, $\varphi(0) = 0$, and Lipschitz continuous with Lipschitz constant L: $\left|\varphi(v) - \varphi\left(\hat{v}\right)\right| \leqslant L\left\|v - \hat{v}\right\|$ for all $v, \hat{v} \in \mathbb{R}^n$. There exist constants λ_{2i} $(i = 1, 2, 3, 4)$, β_2, and positive continuous differentiable function $V_2, W_2 : \mathbb{R}^{n+1} \to \mathbb{R}$ such that

$$\lambda_{21}\|v\|^2 \leqslant V_2(v) \leqslant \lambda_{22}\|v\|^2, \lambda_{23}\|v\|^2 \leqslant W_2(v) \leqslant \lambda_{24}\|v\|^2 \tag{61}$$

$$\sum_{i=1}^{n-1} v_{i+1}\frac{\partial V_2(v)}{\partial v_i} + \varphi(v_1, v_2, \ldots, v_n)\frac{\partial V_2(v)}{\partial v_n} \leqslant -W_2(v) \tag{62}$$

$$\left|\frac{\partial V_2(v)}{\partial v_n}\right| \leqslant \beta_2 \|v\|, \quad \forall v = (v_1, v_2, \ldots, v_n) \in \mathbb{R}^n \tag{63}$$

The Assumption 4 is for TD in (54).

Assumption 4: Both $\upsilon(t)$ and $\dot{\upsilon}(t)$ are bounded in $[0, \infty)$, and $\psi(\cdot)$ is locally Lipschitz continuous, and system (54) with $\upsilon(t) \equiv 0, R \equiv 1$ is globally asymptotically stable.

Theorem 5: Let $\widehat{x}_i(t)$ $(1 \leqslant i \leqslant n)$ and $(1 \leqslant i \leqslant n+1)$ be the solutions of closed-loop system combined of (51) (52). Let $\widehat{x}^*_{n+1}(t)$ be the extended state defined in (52), and let $z_{1R}(t)$ be the solution of (54). Under Assumptions A1-A4, the following statements hold true for any given initial values of (51) and the closed-loop system.

(1) For any $\sigma > 0$ and $\tau > 0$, there exists a constant $R_0 > 0$ such that $|z_{1R}(t) - v(t)| < \sigma$ uniformly in $t \in [\tau, \infty)$ for all $R > R_0$.

(2) For every $R > R_0$, there are an R-dependent constant $\varepsilon_0 > 0$ for any $\varepsilon \in (0, \varepsilon_0)$, and an $\varepsilon-$ dependent constant $t_\varepsilon > 0$ such that for all $t > t_\varepsilon$,

$$\left|\widehat{x}_i(t) - \widehat{x}^*_i(t)\right| \leqslant \Gamma_1 \varepsilon^{n+2-i}, \quad i = 1, 2, \ldots, n+1$$

and

$$\left|\widehat{x}_i(t) - z_{iR}(t)\right| \leqslant \Gamma_2 \varepsilon, \quad i = 1, 2, \ldots, n$$

where Γ_1 and Γ_2 are R-dependent positive constants only.

APPENDIX B
NUMERICAL ANALYSIS

If let $\hat{b}_0 = 2011$, $k_p = 0.014$, $k'_p = 12$, $k'_i = 2.3$. Then the Lipschitz continuous function $\varphi(x_1, x_2, x_3)$ is

$$\varphi(x_1, x_2, x_3) = -64.8x_1 - 337.8x_2 - 28.1x_3 \tag{64}$$

And

$$A = \begin{bmatrix} 0 & 1 & 0 \\ 0 & 0 & 1 \\ -64.8 & -337.8 & -28.1 \end{bmatrix}$$

$$P_A = \begin{bmatrix} 2.9676 & 1.3827 & 0.0077 \\ 1.3827 & 6.2266 & 0.0056 \\ 0.0077 & 0.0056 & 0.0180 \end{bmatrix}$$

So, the Lyapunov function is

$$\begin{aligned} V(x) &= 2.9676x_1^2 + 6.2266x_2^2 + 0.0180x_3^2 \\ &\quad + 2.7654x_1x_2 + 0.0154x_1x_3 + 0.0112x_2x_3 \end{aligned} \tag{65}$$

$$\begin{aligned} V(x) &= 2.9676x_1^2 + 6.2266x_2^2 + 0.0180x_3^2 \\ &\quad + 2.7654x_1x_2 + 0.0154x_1x_3 + 0.0112x_2x_3 \\ &\geqslant 1.3772x_1^2 + 4.8383x_2^2 + 0.0047x_3^2 \\ &\geqslant 0.0047\left(x_1^2 + x_2^2 + x_3^2\right) = \lambda_{21}\|x\|^2 \end{aligned} \tag{66}$$

TABLE 4. Nomenclatures.

Symbol	Description
J_M	Motor inertia
J_L	Load inertia
K_S	Stiffness of the shaft
b_s	Damping ratio
T_M	Electromagnetic torque of the motor
T_L	Load torque
ω_M,x_2	Speed of the motor
θ_M,x_1,y	Angle of the motor
ω_L	Speed of the load
θ_L	Angle of the load
I_{ref}	Reference motor current
k_T	Torque coefficient of the motor
ω_A	Anti-resonant frequency
ω_N	Resonant frequency
T_f	Time constant of current loop
w	External disturbance
b_0	k_T/J_M
f,f_0,x_3	Total disturbance
k_p	Speed controller proportional gain of ADRC
u_0	Virtual control signal
u	Compensated control signal
ε_1	Observer error
β_{01},β_{02},β_{03}	Observer gains
$\hat{b}_0$	Estimated value of b_0
δ	Parameter to be tuned
z_1,z_2,z_3	Observer states tracking θ_M, ω_M,f
k'_p	Proportional gain of PI position controller
k'_i	Integral coefficient of PI position controller
T_D	Time constant of the low-pass filter
$\nu(k)$	Reference input of NTD
$\tilde{x}_1(k)$,$\tilde{x}_2(k)$	State tracking $\nu(k)$ and $\tilde{x}_1(k)$
h	Sampling interval of NTD
h_0,d,d_0,y_1,a_0,a_1	Intermediate variables of NTD
r	Speed factor of NTD
ω_{TD}	Bandwidth of NTD
θ_{ref}	Reference position
$\theta_{ref\_f}(k)$	The state tracking $\theta_{ref}(k)$
$\omega_f(k)$	Feedforward speed
$\omega_{ref\_f}(k)$	State tracking $\omega_f(k)$
$a_f(k)$	Feedforward acceleration
K_ω	Feedforward speed coefficient
K_a	Feedforward acceleration coefficient
$\tilde{z}_1$,$\tilde{z}_2$	Observer states tracking ω_M and f_0
$\tilde{\beta}_{01}$,$\tilde{\beta}_{02}$	Observer gains of LESO
ω_o	Observer bandwidth of LESO
ω_{cross}	The intersection point of $f_{LESO}(s)$ and $f_{AFC}(s)$
r_o	Observer bandwidth of the acceleration observer
a	Feedback gain of AFC
k_{ap},k_{ai},k_{ad}	Parameters of the Luenberger acceleration observer
k_{sp},k_{si}	Parameters of the speed controller of AFC
k_{pp},k_{pi}	Parameters of the position controller of AFC
k'_p,k'_i	Position controller proportional gain of ADRC
T_F	Friction torque

$$\begin{aligned} V(x) &= 2.9676x_1^2 + 6.2266x_2^2 + 0.0180x_3^2 \\ &\quad + 2.7654x_1x_2 + 0.0154x_1x_3 + 0.0112x_2x_3 \\ &\leqslant 4.1580x_1^2 + 7.6149x_2^2 + 0.0313x_3^2 \\ &\leqslant 7.6149\left(x_1^2 + x_2^2 + x_3^2\right) = \lambda_{23}\|x\|^2 \end{aligned} \tag{67}$$

$$\begin{aligned} &\sum_{i=1}^{2} x_{i+1}\frac{\partial V}{\partial x_i} - \left(\hat{b}_0 k_p k'_i x_1 + \hat{b}_0 k_p k'_p x_2 + \hat{b}_0 k_p x_3\right)\frac{\partial V}{\partial x_3} \\ &\quad = -{x_1}^2 - {x_2}^2 - {x_3}^2 = -\langle x, x\rangle = -W(x) \end{aligned} \tag{68}$$

So Assumption 3 is satisfied.

APPENDIX C
NOMENCLATURE

See Table 4.

REFERENCES

[1] M. Garcia-Sanz, T. Ranka, and B. C. Joshi, "High-performance switching QFT control for large radio telescopes with saturation constraints," in *Proc. IEEE Nat. Aerosp. Electron. Conf. (NAECON)*, Dayton, OH, USA, Jul. 2012, pp. 84–91.

[2] W. Gawronski, B. Bienkiewicz, and R. E. Hill, "Wind-induced dynamics of a deep space network antenna," *J. Sound Vib.*, vol. 178, no. 1, pp. 67–77, 1994.

[3] W. Gawronski and K. Souccar, "Control systems of the large millimeter telescope," *IEEE Antennas Propag. Mag.*, vol. 47, no. 4, pp. 41–49, Aug. 2005.

[4] D. Qiu, M. Sun, Z. Wang, Y. Wang, and Z. Chen, "Practical wind-disturbance rejection for large deep space observatory antenna," *IEEE Trans. Control Syst. Technol.*, vol. 22, no. 5, pp. 1983–1990, Sep. 2014.

[5] G. Ellis and Z. Gao, "Cures for low-frequency mechanical resonance in industrial servo systems," in *Proc. IEEE Ind. Appl. Conf. 36th IAS Annu. Meeting*, Chicago, IL, USA, Sep./Oct. 2001, pp. 252–258.

[6] B. Sedghi, B. Bauvir, and M. Dimmler, "Acceleration feedback control on an AT," *Proc. SPIE*, Jul. 2008, Art. no. 70121Q.

[7] W. Gawronski, "Control and pointing challenges of large antennas and telescopes," *IEEE Trans. Control Syst. Technol.*, vol. 15, no. 2, pp. 276–289, Mar. 2007.

[8] S. J. Dyke, B. F. Spencer, P. Quast, M. K. Sain, D. C. Kaspari, and T. T. Soong, "Acceleration feedback control of MDOF structures," *J. Eng. Mech.*, vol. 122, no. 9, pp. 907–918, 1996.

[9] E. Dumetz, J. Y. Dieulot, P. J. Barre, F. Colas, and T. Delplace, "Control of an industrial robot using acceleration feedback," *J. Intell. Robotic Syst.*, vol. 46, no. 2, pp. 111–128, Jul. 2006.

[10] A. M. Higginson, S. Sanders, and C. Wallett, "Estimated acceleration feedback applied to a telescope servo system," *Mechatronics*, vol. 1, no. 4, pp. 509–523, Jan. 1991.

[11] M. Suárez, J. Rosich, J. Ortega, and A. Pazos, "The GTC main axes servos and control system," *Proc. SPIE*, Jul. 2008, Art. no. 70190J.

[12] Q. Wang, H.-X. Cai, Y.-M. Huang, L. Ge, T. Tang, Y.-R. Su, X. Liu, J.-Y. Li, D. He, S.-P. Du, "Acceleration feedback control (AFC) enhanced by disturbance observation and compensation (DOC) for high precision tracking in telescope systems," *Res. Astron. Astrophys.*, vol. 16, no. 8, p. 1254, 2016.

[13] T. Tang, T. Zhang, J.-F. Du, G. Ren, and J. Tian, "Acceleration feedback of a current-following synchronized control algorithm for telescope elevation axis," *Res. Astron. Astrophys.*, vol. 16, no. 11, p. 165, 2016.

[14] S. Zhao and Z. Gao, "An active disturbance rejection based approach to vibration suppression in two-inertia systems," in *Proc. Amer. Control Conf.*, Baltimore, MD, USA, Jun./Jul. 2010, pp. 1520–1525.

[15] S. Zhao and Z. Gao, "An active disturbance rejection based approach to vibration suppression in two-inertia systems," *Asian J. Control*, vol. 15, no. 2, pp. 350–362, 2013.

[16] Q. Zheng and Z. Gao, "On observer-based active vibration control of two-inertia systems," in *Proc. Amer. Control Conf.*, Washington, DC, USA, Jun. 2013, pp. 6619–6624.

[17] H. Zhang, S. Zhao, and Z. Gao, "An active disturbance rejection control solution for the two-mass-spring benchmark problem," in *Proc. Amer. Control Conf. (ACC)*, Jul. 2016, pp. 1566–1571.

[18] S. Chen, W. Bai, Y. Hu, Y. Huang, and Z. Gao,"On the conceptualization of 'total disturbance' and its profound implications," *Sci. China Inf. Sci.*, vol. 54, pp. 54–146, Apr. 2018.

[19] Y. Chen, B. M. Vinagre, and I. Podlubny, "Fractional order disturbance observer for robust vibration suppression," *Nonlinear Dyn.*, vol. 38, nos. 1–4, pp. 355–367, 2004.

[20] Y. Luo, T. Zhang, B. Lee, C. Kang, and Y. Chen, "Disturbance observer design with Bode's ideal cut-off filter in hard-disc-drive servo system," *Mechatronics*, vol. 23, no. 7, pp. 856–862, 2013.

[21] J. Cui, S. Zeng, Y. Ren, X. Chen, and Z. Gao, "On the robustness and reliability in the pose deformation system of mobile robots," *IEEE Access*, vol. 6, pp. 29747–29756, 2018.

[22] J. Han, "From PID to active disturbance rejection control," *IEEE Trans. Ind. Electron.*, vol. 56, no. 3, pp. 900–906, Mar. 2009.

[23] W. P. Lounsbury and M. Garcia-Sanz, "High-performance quantitative robust switching control for optical telescopes," *Proc. SPIE*, Jul. 2014, Art. no. 91521F.

[24] Y. Chen, M. Yang, J. Long, K. Hu, D. Xu, and F. Blaabjerg, "Analysis of oscillation frequency deviation in elastic coupling digital drive system and robust notch filter strategy," *IEEE Trans. Ind. Electron.*, vol. 66, no. 1, pp. 90–101, Jan. 2019.

[25] Y. Xia, M. Fu, C. Li, F. Pu, and Y. Xu, "Active disturbance rejection control for active suspension system of tracked vehicles with gun," *IEEE Trans. Ind. Electron.*, vol. 65, no. 5, pp. 4051–4060, May 2018.

[26] L. Sun, D. Li, K. Hu, K. Y. Lee, and F. Pan, "On tuning and practical implementation of active disturbance rejection controller: A case study from a regenerative heater in a 1000 MW power plant," *Ind. Eng. Chem. Res.*, vol. 55, no. 23, pp. 6686–6695, 2016.

[27] J. Q. Han and W. Wang, "Nonlinear tracking-differentiator," (in Chinese), *J. Syst. Sci. Math. Sci.*, vol. 2, pp. 177–183, Jul. 1994.

[28] J. Q. Han, *Active Disturbance Rejection Control Technique-the Technique for Estimating and Compensating the Uncertainties*. Washington, DC, USA: National Defense Univ. Press, 2008, pp. 73–75.

[29] Z.-L. Zhao and B.-Z. Guo, "A nonlinear extended state observer based on fractional power functions," *Automatica*, vol. 81, pp. 286–296, Jul. 2017.

[30] B.-Z. Guo and Z.-L. Zhao, "On convergence of tracking differentiator and application to frequency estimation of sinusoidal signals," in *Proc. 8th Asian Control Conf. (ASCC)*, Kaohsiung, Taiwan, May 2011, pp. 1470–1475.

[31] Z.-L. Zhao and B.-Z. Guo, "On convergence of nonlinear active disturbance rejection control for SISO nonlinear systems," *J. Dyn. Control Syst.*, vol. 22, no. 2, pp. 385–412, 2016.

[32] Z. Gao, "Scaling and bandwidth-parameterization based controller tuning," in *Proc. Amer. control Conf.*, Denver, CO, USA, 2003, pp. 4989–4996.

[33] J. Li, Y. Xia, X. Qi, and Z. Gao, "On the necessity, scheme, and basis of the linear–nonlinear switching in active disturbance rejection control," *IEEE Trans. Ind. Electron.*, vol. 64, no. 2, pp. 1425–1435, Feb. 2017.

[34] C. Liu, G. Luo, Z. Chen, W. Tu, and C. Qiu, "A linear ADRC-based robust high-dynamic double-loop servo system for aircraft electro-mechanical actuators," *Chin. J. Aeronaut.*, to be published.

XIN LI received the B.S. and M.S. degrees from the School of Automation, Northwestern Polytechnical University, China, in 2011 and 2014, respectively. He is currently pursuing the Ph.D. degree with the Institute of Optics and Electronics (IOE), Chinese Academy of Sciences (CAS), China. His research interests include robust control, ADRC, and high-precision servo control systems in large telescopes.

WENLIN ZHOU received the B.S. and M.S. degrees from the School of Automation, Northwestern Polytechnical University, China, in 2012 and 2015, respectively. She is currently a Research Associate with the Institute of Optics and Electronics (IOE), Chinese Academy of Sciences (CAS), China. Her research interests include robust control, ADRC, PMSM, and motion control systems.

JUN LUO received the B.S. degree from Northeast Normal University and the Ph.D. degree from the Changchun Institute of Optics, Fine Mechanics and Physics (CIOMP), Chinese Academy of Sciences (CAS), where he is currently a Research Associate with the Institute of Optics and Electronics (IOE). His research interests include high precision sensor and motion control systems.

JUNZHANG QIAN received the B.S. degree from the School of Automation, Northwestern Polytechnical University, China, and the Ph.D. degree from the Institute of Optics and Electronics (IOE), Chinese Academy of Sciences (CAS), China, where he is currently a Research Associate at Institute of Optics and Electronics. His research interests include PMSM, sliding mode control (SMC), and robust control.

WENLI MA graduated from the University of Electronic Science and Technology of China. He is currently a Research Fellow and a Doctoral Supervisor with the Institute of Optics and Electronics (IOE), Chinese Academy of Sciences (CAS), China. His research interests include photoelectric detection, precision machinery, and large photoelectric telescope.

PING JIANG graduated from the Sichuan University, China. He is currently a Research Fellow with the Institute of Optics and Electronics (IOE), Chinese Academy of Sciences (CAS), China. His research interests include photoelectric detection, precision machinery, and large photoelectric telescope.

YONGKUN FAN graduated from the Chang'an University, China. He is currently an Associate Professor with the Sichuan Vocational and Technical College of Communications. His research interests include PMSM, new energy electric vehicles, and robust control.